ACS Partner Journal
CHEM & BIO ENGINEERING
pubs.acs.org/ChemBioEng

Article

Antiviral Rotenoids and Isoflavones Isolated from *Millettia oblata ssp. teitensis*

Kiganda Bogaerts Wieske Deyou Atilaw Uwamariya Miah Said Ndakala Akala Herrebout Trybala Bergström Yenesew Erdelyi[†,‡,' ;‡;' ;‡; ;§;§;§;†;Δ;' ;§;§,*;†,;*;‡,;*]

Cite This: default. 2024, 0

ABSTRACT: Three new (**1-3**) and six known rotenoids (**5-10**), along with three known isoflavones (**11-13**), were isolated from the leave *Millettia oblata* ssp. *teitensis*. A new glycosylated isoflavone (**4**), four known isoflavones (**14-18**) and one known chalcone (**19**) were isolated from the root wood extract of the same plant. The structures were elucidated by NMR spectroscopic and mass spectrometric analyses. The absolute configuration of the chiral compounds was established by comparison of experimental ECD and VCD data with those calculated for the possible stereoisomers. This the first report on the use of VCD to assign the absolute configuration of rotenoids. The crude leaves and root wood extracts displayed anti-RSV (human respiratory syncytial virus) activity with IC_{50} values 0.7 μg/mL and 3.4 μg/mL, respectively. Compounds **6**, **8**, **10**, **11**, and **14** showed anti-RSV activity with IC_{50} values 0.4 - 10 μM, while compound **3** exhibited anti-HRV-2 (human rhinovirus 2) activity with IC_{50} of 4.2 μM. Most of the compounds showed low cytotoxicity for laryngeal carcinoma (HEp-2) cells, however compounds **3**, **11**, and **14** exhibited low cytotoxicity also in primary lung fibroblasts. This is the first report on rotenoids showing antiviral activity against RSV and HRV viruses.

RESULTS AND DISCUSSION

The CH_2Cl_2/MeOH (1:1) extract of the leaves of *Millettia oblata* ssp. *teitensis* was subjected to a silica gel column chromatography, followed by purification by Sephadex LH-20 and preparative thin layer chromatography (TLC) to afford the three new rotenoids oblarotenoid E (**1**), oblarotenoid F (**2**), and oblarotenoid G (**3**). Similar treatment of the root wood afforded the new isoflavone glycoside, obloneside (**4**), the six known rotenoids oblarotenoid C (**5**),[18] oblarotenoid A (**6**),[18] oblarotenoid D (**7**),[18] 12a-hydroxymunduserone (**8**),[18] tephrosin (**9**),[23] and deguelin (**10**),[17] the seven known isoflavones ichthynone (**11**),[24] 7,2' ,5' -trimethoxy-3' ,4' -methylenedioxyisoflavone (**12**),[18] isoerythrin-A-4' -prenyl ether (**13**),[25] 4' -prenyloxyderrone (**14**),[26] aglycuneatin methyl ether (**15**),[27] calopogonium isoflavone B (**16**),[28] maximaisoflavone G (**17**)[17] and milldurone (**18**)[27] and the known chalcone isobavachromene (**19**).[29] The known compounds were identified by comparison of the experimental spectroscopic data to literature data (Supporting information). The ^{13}C NMR assignment of compounds **1-4** was confirmed by CSEARCH.[30]

Compound **1** was obtained as a white amorphous solid that showed UV absorption maxima at 280 and 305 nm. Its molecular formula was established as $C_{19}H_{16}O_7$ based on HRESIMS ($[M+H]^+$ at m/z 357.0976, calcd for $C_{19}H_{17}O_7$ 357.0974, Figures S1-S8, Supporting Information) and NMR data (Table 1). The ^1H NMR spectrum displayed four sets of coupled aliphatic protons at δ_H 4.21 (br d, J =12.1 Hz, H-6), 4.65 (dd, J =12.1, 3.0 Hz, H-6), 4.94 (m, H-6a), and δ_H 3.81 (H-12a, overlapping with a OMe signal), which are consistent with the NMR signals expected for the B ring of a rotenoid skeleton.[31] The ^{13}C NMR spectrum displayed the corresponding signals at δ_C 66.8 (C-6), 72.7 (C-6a), 189.0 (C-12), and 45.0 (C-12a). Two methoxy (δ_H 3.71 and 3.81; δ_C 57.2 and 56.2) and a methylenedioxy group (δ_H 5.91 and δ_H 5.97; δ_C 102.7) were also identified, based on their characteristic chemical shifts. The three mutually coupled aromatic protons of ring D showed an AMX spin system at δ_H 7.85 (d, J = 8.9 Hz, H-11), δ_H 6.59 (dd, J = 8.9, 2.3 Hz, H-10), and δ_H 6.44 (d, J = 2.3 Hz, H-8) (Table 2 and Figures S1-S8, Supporting information). The placement of the methoxy group at C-9 (δ_C 167.0) was supported by the HMBC cross peaks from H-8 (δ_H 6.44), H-10 (δ_H 6.59), and H-11 (δ_H 7.85) to C-9 (δ_C 167.0), and from OMe-9 (δ_H 3.85) to C-9. The OMe-9 group further showed NOE correlation to H-8 (δ_H 6.44). This substitution pattern is consistent with the biogenetically expected oxygenation (OMe) at C-9.[32] The remaining aromatic proton (δ_H 6.39) was assigned to H-1, based on its HMBC correlations with C-1a (δ_C 109.4), C-4a (δ_C 133.2), and C-12a (δ_C 45.0). This places the second methoxy and the methylenedioxy groups at C-2, C-3, and C-4, giving rise to two alternative structures that have the methoxy group at C-2 or at C-4. The observed ^{13}C NMR chemical shift of the methoxy (δ_C 57.2) better fits to oxygenation at C-2 as it would be expected to have a chemical shift above 59 ppm if it was at C-4, due to di-*ortho* substitution.[33] The placement of the methoxy group at C-2 (δ_C 138.9) was further supported by the NOE correlation between OMe-2 (δ_H 3.73) and H-1

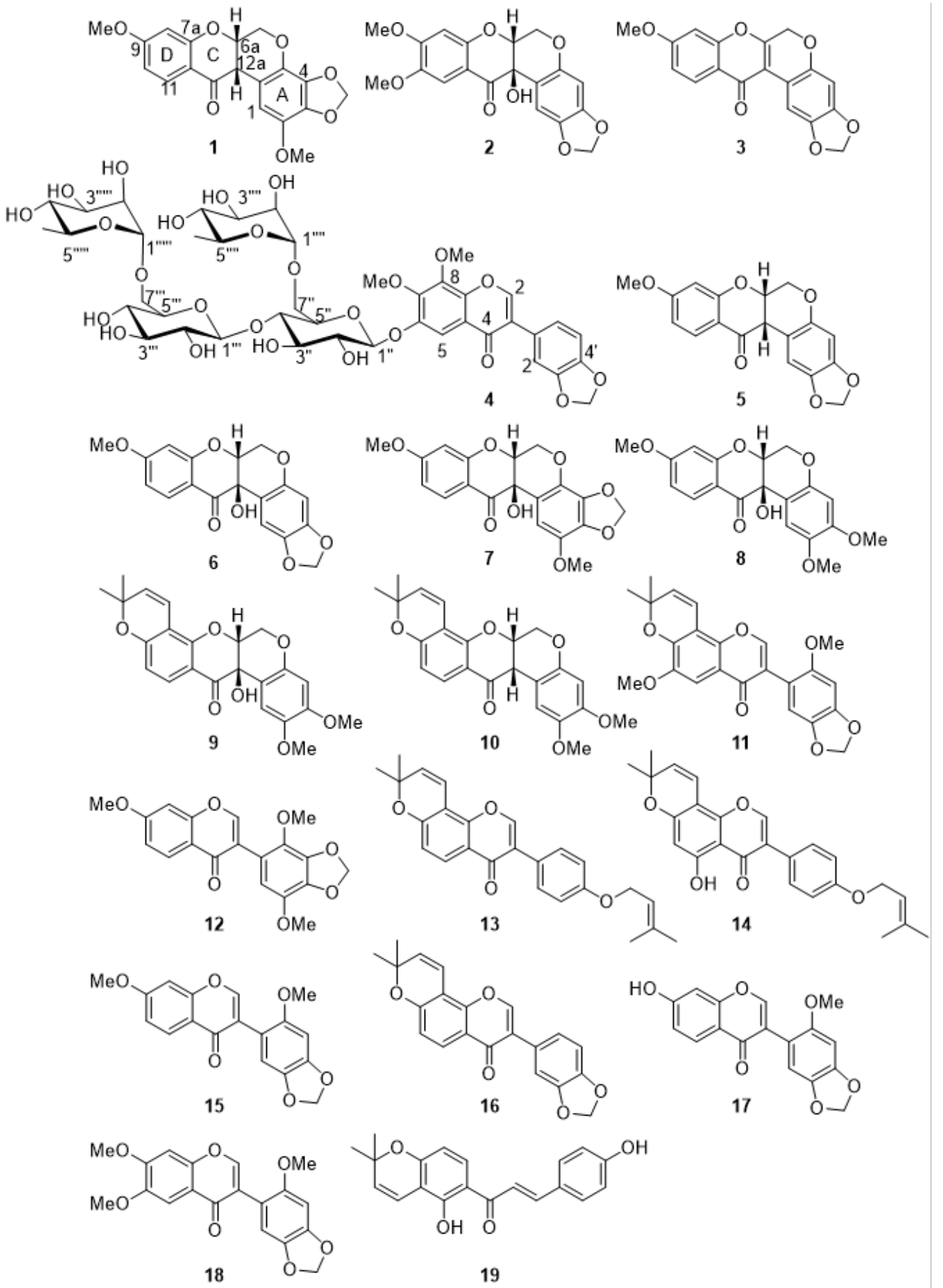
1
2
3
4
5
6
7
8
9
10
11
12
13
14
15
16
17
18
19

(δ_H 6.31), and by the HMBC correlations of H-1 (δ_H 6.31) with C-1a (δ_C 109.4), C-2 (δ_C 138.9), C-3 (δ_C 136.3),

[a] CD_2Cl_2 was used due to gradual color change observed in the slightly acidic $CDCl_3$; [b] HMBC correlations, optimized for 6 Hz, are from the stated proton(s) to the indicated carbon; [c] Signal overlapping with that of OMe-9

C-4a (δ_C 133.2), and C-12a (δ_C 45.0) as well as between OMe-2 (δ_H 3.73) and C-2 (δ_C 138.9) (Table 1). Based on the spectroscopic data, the gross structure of compound **1** was identified as 2,9-dimethoxy-3,4-methylenedioxyrotenoid. It has an uncommon trisubstitution with a methoxy and a methylenedioxy group at its ring A, which may indicate it to be biosynthesised from 7,2',5'-trimethoxy-3' ,4' -methylenedioxyisoflavone (**12**), a co-metabolite that has the same oxygenation pattern in its B-ring as the A-ring of **1**. The chemical shift of H-1 (δ_H 6.39) along with the small coupling constant (J = 2.9 Hz) between H-6 (δ_H 4.65 and 4.21) and H-6a (δ_H 4.94) suggested that H-6a is equatorially oriented and compound **1** hence has a *cis*-configuration at its B/C ring junction, which has been reported as the thermodynamically most favorable configuration.[18] The NOE correlation between H-6a (δ_H 4.94) and H-12a (δ_H 3.81) corroborates the *cis* configuration of the B/C ring junction. To determine the absolute configuration, the ECD spectrum of **1** was recorded (Figure 1). According to Slade *et al.* (2005), dextrorotatory rotenoids with *cis*-B/C ring junction, showing positive Cotton Effect (CE) at 300-330 nm (πR to π^* transition) and negative CE at 348-360 nm (for n to π^* transition), are associated with (6a,12a*R*) configuration. On the other hand, levororotatory rotenoids with *cis*-B/C ring junction, showing negative CE at 300-330 nm, and a positive CE at 348-360 nm, are associated with (6a*S*,12a*S*) configuration. The n to π^* transition at 348-360 nm is generally weak and for many rotenoids it has not been observed, and thus may not be a reliable indicator for determination of rotenoids' absolute configuration.[18] Compound **1** is dextrorotatory with a $[\alpha]^{20}_D$ +44.0 (*c* 0.2 CH_3OH), and showed a negative CE at 330 nm for its π to π^* transition in its ECD spectrum. This contradicts the above literature proposal.[34] Similar contradiction has previously been reported for some rotenoids, which had either low positive or low negative specific rotation.[18] In contrast to prenylated rotenoids with *cis*-B/C ring junction that show specific rotations $[\alpha]^{20}_D$ < -100 or $[\alpha]^{20}_D$ > +100, with the sign of the rotation reliably indicating the absolute configuration,[35-36] non-prenylated rotenoids with *cis*-B/C ring junction typically show specific rotations -50 < $[\alpha]^{20}_D$ < +50, and the sign of the rotation is not reliable for determining their absolute configuration.[18] For compound **1**, which has a positive specific rotation of $[\alpha]^{20}_D$ +44.0 (*c* 0.2 CH_3OH), we relied on the ECD spectrum and assigned its absolute configuration as (6a*S*,12a*S*)-**1** upon comparison of its ECD spectrum with that reported for (6a*S*,12a*S*)-9-methoxy-2,3-methylenedioxyrotenoid, a related rotenoid whose absolute configuration was established by single-crystal X-ray crystalography.[34] The absolute configuration of compound **1** was confirmed by acquiring a VCD spectrum (Figure 2), which showed a good match with that simulated for the (6a*S*,12a*S*) stereoisomer of **1**, whereas showed no match for the predicted spectrum of the (6a*S*,12a*R*) stereoisomer. The vibrational IR pattern of **1** at 1300-1200 cm^{-1} (Figure S135, Supporting Information) was further consistent with *cis* configuration at the B/C ring junction.[37-38] This is the first report of the use of

VCD spectroscopy to determine the relative and the absolute configuration of rotenoids. Based on the spectroscopic data, the new compound (**1**) was identified as (6a*S*,12a*S*)-2,9-dimethoxy-3,4-methylenedioxyrotenoid, and was given the trivial name oblarotenoid E. It is structurally closely related to the previously reported oblarotenoid C,[18] differing in the substitution of its ring A.

Compound **2** was isolated as a white amorphous solid. Its molecular formula was established as $C_{19}H_{16}O_8$ based on MS ($[M+H]^+$ at *m/z* 373.2) and HRESIMS data ($[M+H-H_2O]^+$ at *m/z* 355.0354) consistent with the formula $C_{19}H_{15}O_7$ (calcd 355.0818); and NMR data (Table 1). The UV absorbance at λ_{max} 285 and 305 nm as well as the ^1H NMR [δ_H 4.58 dd, J = 13.5, 2.6 Hz (H-6), 4.46, dd J = 13.5, 2.6Hz (H-6), and 4.56, d, J = 3.6 Hz (H-6a)] and ^{13}C NMR [(δ_C 64.6 (C-6), 76.4 (C-6a), 191.3 (C-12) and 67.9 (C-12a)] data (Table 1, Figures S10-S17, Supporting information) were consistent with a 12a-hydroxyrotenoid skeleton.[18] The NMR spectra indicated a methylenedioxy (δ_H 5.83 and 5.86; δ_C 101.5) and two methoxy (δ_H 3.86 and 3.88; δ_C 56.4 and 56.5) functionalities. The four singlet aromatic protons H-1 (δ_H 6.54), H-4 (δ_H 6.46), H-8 (δ_H 6.40), and H-11 (δ_H 7.25) were consistent with C-2, C-3, C-9, and C-10 oxygenation of the 12a-hydroxyrotenoid skeleton. The NOE correlation of H-11 (δ_H 7.25) with OMe-10 (δ_H 3.88), and the NOE of OMe-9 (δ_H 3.86) with H-8 (δ_H 6.40) along with the HMBC of H-8 (δ_H 6.40) to C-7a (δ_C 157.5), C-9 (δ_C 157.3), C-10 (δ_C 149.5), and C-11a (δ_C 109.5) as well as of H-10 (δ_H 6.59) to C-8 (δ_C 100.3), C-9 (δ_C 157.3), and C-11a (δ_C 109.5) placed the two OMe groups of ring D at C-9 (δ_C 145.3) and C-10 (δ_C 157.3), respectively. The methylenedioxy moiety was placed at C-2/C-3 based on the HMBC correlations of H-1 (δ_H 6.54) to C-1a (δ_C 109.9), C-2 (δ_C 109.9), C-3 (δ_C 109.9), C-4a (δ_C 149.5), and C-12a (δ_C 67.9), as well as of H-4 (δ_H 6.46) to C-1a (δ_C 109.9), C-2 (δ_C 109.9) and C-3 (δ_C 109.9), leading to the planar structure 9,10-dimethoxy-2,3-methylenedioxy-12a-hydroxyrotenoid for compound **2**. The chemical shift of H-1 (δ_H 6.54) along with the small coupling constants, $J \leq 3.3$ Hz, between H-6a (δ_H 4.59) and the CH_2-6 protons (δ_H 4.58 and 4.46) indicated a *cis* B/C ring junction,[34] whereas the negative Cotton effect at *ca.* 340 nm suggested a (6a*R*,12a*R*)-**2** absolute configuration.[18] Similar to compound **1**, the positive specific rotation $[\alpha]^{20}_D$ +42° (*c* 0.3 CH_3OH) was not found reliable in assigning the configuration of **2**. Instead, its (6a*R*,12a*R*)-**2** absolute configuration was determined by the comparison of its experimental VCD (Figure 3) with calculated spectra. This configuration was corroborated by the IR band pattern between 1350 cm^{-1} and 1000 cm^{-1} (Figure S136, Supporting Information), which indicated a *cis* configuration.[37-38] Based on the spectroscopic data, the new compound **2** was identified as (6a*R*,12a*R*)-9,10-dimethoxy-2,3-methylenedioxy-12a-hydroxyrotenoid, and was given the trivial name oblarotenoid F. It is structurally closely related to the previously reported oblarotenoid A,[18] differing in the substitution of its ring D. It should be emphasized that despite structural similarities, the specific rotation of oblarotenoid F, $[\alpha]^{20}_D$ +42°, has an opposite sign as compared to those of oblarotenoid A, $[\alpha]^{20}_D$ -38.3°,

Table 1. NMR Spectroscopic Data (^{1H} 500 and ^{13C} 125 MHz) of Oblarotenoids E (1), F (2) (CD_2Cl_2[a]), and G ($CDCl_3$)

	1			2			3		
position	δ_C, type	δ_H (J in Hz)	HMBC[b]	δ_C, type	δ_H (J in Hz)	HMBC	δ_C, type	δ_H (J in Hz)	HMBC
1	106.6, CH	6.31 s	C-1a, C-2, C-3, C-4a, C-12a	105.9, CH	6.54 s	C-1a, C-2, C-3, C-4a, C-12a	107.1, CH	8.32 s	C-2, C-3, C-4a, C-12a
1a	109.4, C			109.9, C			111.8, C		
2	138.9, C			149.5, C			142.9, C		
3	136.3, C			142.4, C			147.4, C		
4	136.9, C			99.3, CH	6.46 s	C-1a, C-2, C-3	98.7, CH	6.53 s	C-1a, C-2, C-3
4a	133.2, C			149.5, C			147.5, C		
6	66.8, CH_2	4.65 dd (12.5, 2.6)	C-4a, C-6a, C-12a	64.0, CH_2	4.58 dd (13.5, 2.6)	C-4a, C-6a, C-12a	65.0, CH_2	4.96 s	C-4a, C-6a, C-12a
		4.21 br d (12.5)	C-4a,C-6a		4.46 d (13.5,2.6)	C-4a,C-6a			
6a	72.7, CH	4.94 dd (2.6)	C-1a, C-4a, C-6, C-12, C-12a	76.4, CH	4.56 br d (3.6)	C-1a, C-4a, C-6, C-12, C-12a	156.8, C		
7a	163.0, C			157.5, C			156.7, C		
8	100.9, CH	6.44 d (2.3)	C-7a, C-9, C-10, C-11a	100.3, CH	6.40 s	C-7a, C-9, C-10, C-11a	100.3, CH	6.83 d (2.2)	C-7a, C-9, C-10, C-11a
9	167.0, C			157.3, C			164.0, C		
10	110.9, CH	6.59 dd (8.9, 2.3)	C-8, C-9, C-11a	145.3, C		C-8, C-9, C-11a	114.7, CH	7.00 dd (8.9, 2.2)	C-8, C-11a
11	129.6, CH	7.85 d (8.9)	C-7a, C-9, C-12	106.9, CH	7.25 s	C-7a, C-9, C-12	127.9, CH	8.20 d (8.9)	C-7a, C-9, C-12
11a	113.1, C			109.5, C			118.7, C		
12	189.0, CO			191.3, CO			174.2, CO		
12a	45.0, CH	3.81[c]	C-1a, C-4, C-6	67.9, C			112.3, C		
OCH_2O	102.7, CH_2	5.97 d (1.4);	C-3, C-4	101.5, CH_2	5.83 d (1.4); 5.86 d (1.4)	C-2, C-3	101.5, CH_2	5.96 s	C-2, C-3
		5.91 d (1.4)							
OMe-2	57.2, CH_3	3.73 s	C-2	-	-	-	-	-	-
OMe-9	56.2, CH_3	3.81 s	C-9	56.4, CH_3	3.86 s	C-9	56.0, CH_3	3.92 s	C-9
OMe-10	-	-	-	56.5, CH_3	3.88 s	C-10	-	-	-

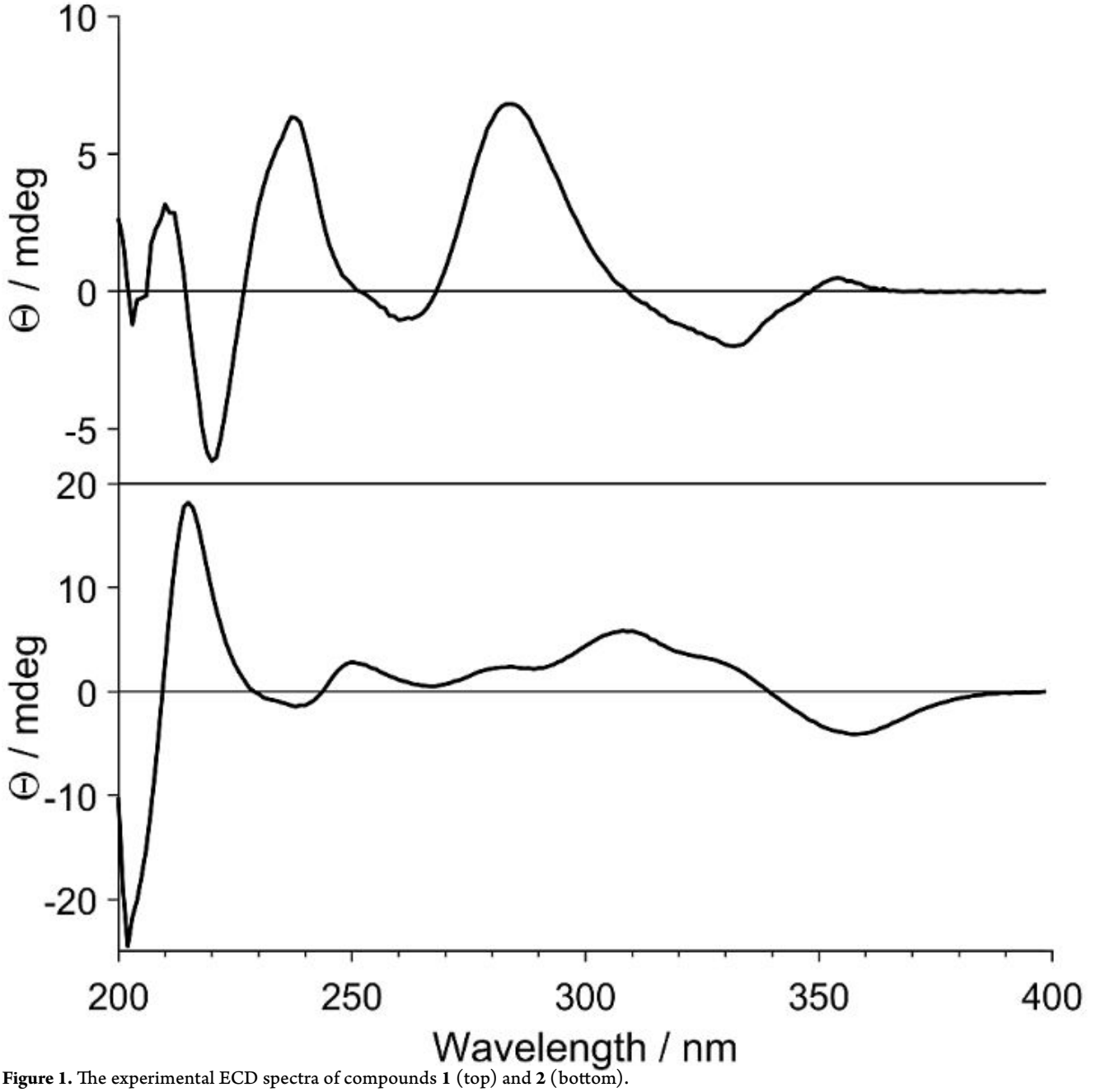

Figure 1. The experimental ECD spectra of compounds **1** (top) and **2** (bottom).

and of (-)-(6a*R*,12a*R*)-12a-hydroxy-α-toxicarol, $[\alpha]^{20}_{D}$ -108°, recently reported from *Millettia brandisiana*.[39] The ECD and the specific rotation data of rotenoids may not be complementary, which has been previously pointed out.[7]

Compound **3** was isolated as a light yellow solid. Its molecular formula, $C_{18}H_{12}O_6$ was established based on HRESIMS ($[M+H]^+$ *m/z* 325.0714, calcd 325.0712) and NMR data (**Table 1**, Figures S18-S24 Supporting Information). UV absorptions at λ_{max} 237 nm, 278 nm, and 310 nm along with the NMR data, especially the chemical shifts of the oxygenated methylene protons H-6 (δ_H 4.96) and of C-6a (δ_C 156.8), suggested **3** to have a 6a,12a-dehydrorotenoid skeleton. Furthermore, typical for 6a,12a-dehydrorotenoids, the deshielded chemical shift of the singlet signal at δ_H 8.32 was assigned to H-1 of ring A.[40] This is due to the magnetic anisotropy of the nearby carbonyl C-12 (δ_C 174.2) and the flat geometry of the molecule [(sp^2 hybridized C-6a (δ_C 156.8) and C-12a (δ_C 112.3)]. The NMR data further indicated the presence of a methoxy (δ_H 3.92, δ_C 56.0) and a methylenedioxy (δ_H 5.96, δ_C 101.5) moieties. Here, the appearance of the two singlets H-1 (δ_H 8.32) and H-4 (δ_H 6.53) was indicative of the placement of the methylenedioxy moiety at C-2/C-3 of ring A, which was further supported by the HMBCs between the methylenedioxy protons (δ_H 5.96) and C-2 (δ_C 142.9) and C-3 (δ_C 147.4). The placement of the methoxy group at C-9 was established upon the presence of three mutually coupled protons H-11 (δ_H 8.20, *d*, *J* = 8.9 Hz), H-10 (δ_H 7.0, dd, *J* = 2.2, 8.9 Hz), and H-8 (δ_H 6.83, d, *J* = 2.2 Hz) in ring D. This was further supported by the HMBCs of the OMe-9

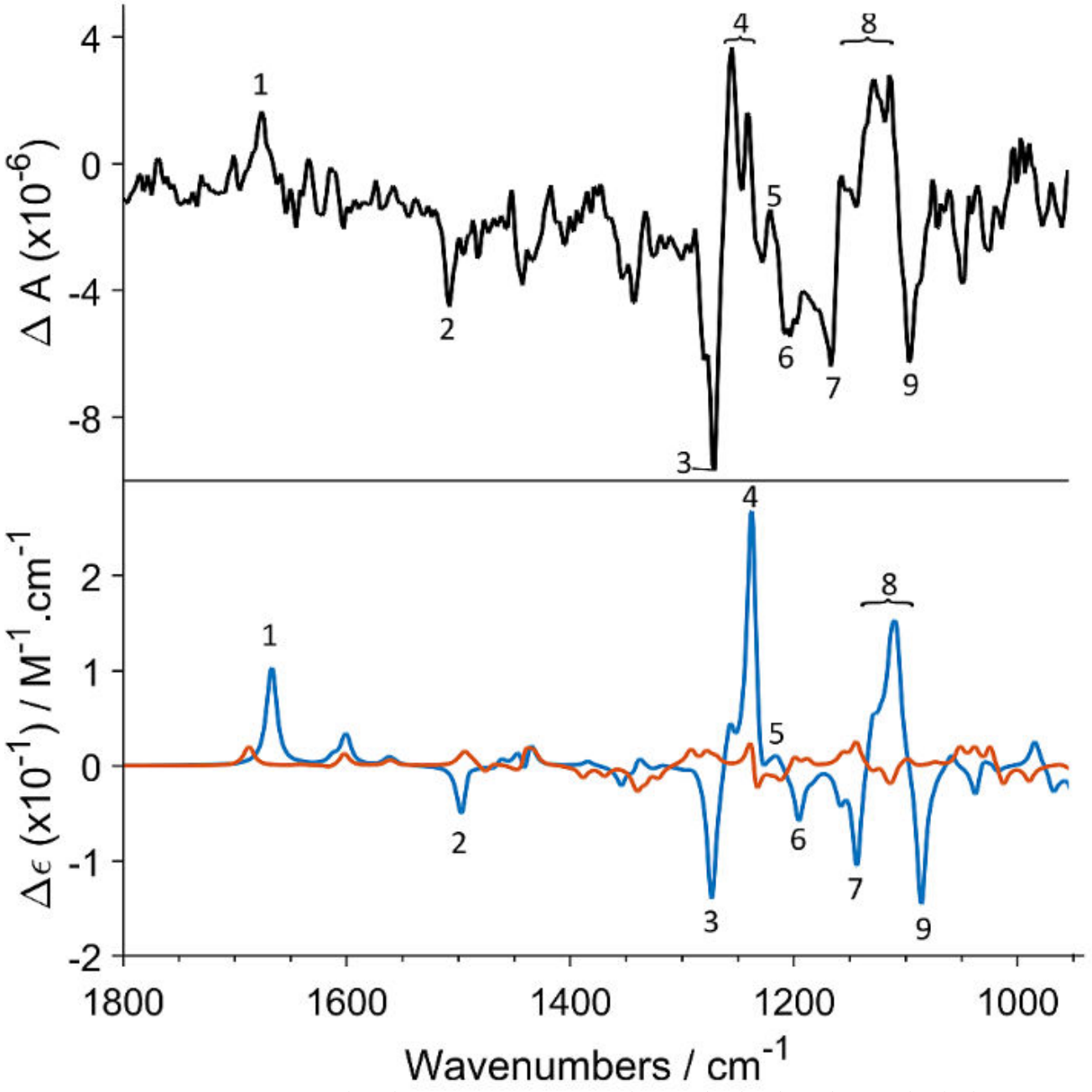

Figure 2. The VCD spectra observed for **1** (black), and those predicted for its (6a*S*,12a*S*)-**1** (blue) and (6a*S*,12a*R*)-**1** (red) stereoisomers. The numbers 1-9 indicate band assignment of key importance for AC assignment, and are given to facilitate comparison of the experimental and simulated spectra.

(δ_H 3.92) to C-9 (δ_C 164.0), of H-11 (δ_H 8.20) to C-9 (δ_C 164.1) and C-12 (δ_C174.2), and of H-8 (δ_H 6.83) to C-7a (δ_C 156.7) and C-11a (δ_C 118.7) as well as by the NOE between OMe-9 (δ_H 3.92) and H-8 (δ_H 6.83). Therefore, the new compound **3** was identified as 9-methoxy-2,3-methylenedioxy-6a-2a-dehydrorotenoid and was given the trivial name oblarotenoid G. It has previously been reported as a synthetic product.[41] Here, we report it as a natural product and provide its the complete NMR data for the first time. It is a structurally close to the previously reported oblarotenoid A,[18] and may be obtained by its dehydration. Oblarotenoid G has been observed in the crude extract, by TLC profiling, confirming that it is not an isolation artefact.

Compound **4** was isolated as a white amorphous solid and was assigned the molecular formula $C_{45}H_{54}O_{25}$ based on HRESIMS ($[M+H]^+$ *m/z* 959.3043) and NMR data (Table 2, Figures S25-S32, Supporting Information). The NMR spectra showed signals at δ_H 8.17 (s, H-2), δ_C 154.2 (C-2), 126.9 (C-3), and 177.1 (C-4) characteristic for an isoflavone[18] substituted with a methylenedioxy (δ_H 5.98, δ_C 102.5), two methoxy (δ_H 3.91; δ_C 62.3 and δ_H 3.92; δ_C 62.8) and sugar moieties. Based on the HMBC of H-5 (δ_H 7.12) to C-4 (δ_C 177.1), C-8a (δ_C 155.5), and C-7 (δ_C 142.1), the single aromatic proton of the trisubstituted ring A was placed at C-5 (δ_C 101.8). Its positioning was confirmed by the HMBC of H-5 (δ_H

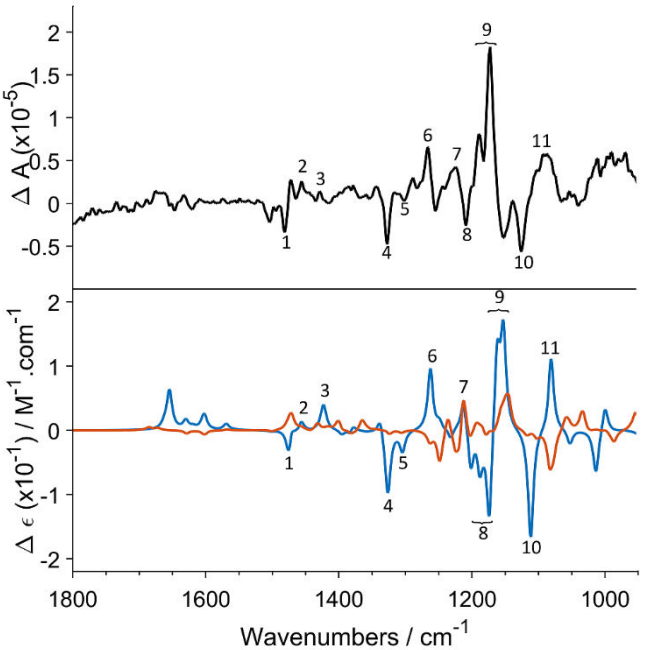

Figure 3. The experimental VCD spectrum of **2** (black), and the spectra predicted for (6a*R*,12a*R*)-**2** (blue) and (6a*R*,12a*S*)-**2** (red). The numbers 1-11 indicate band assignment of key importance for AC assignment, and are given to facilitate comparison of the experimental and simulated spectra.

7.1) to C-4 (δ_C 177.1). The chemical shift values δ_C 62.8 and δ_C 62.3 of the two OMe groups indicated that both are di-*ortho*-disubstituted.[33] They were placed at C-7 and C-8 based on the HMBC of 7-OMe (δ_H 3.92) and C-7 (δ_C 142.1) as well as between 8-OMe (δ_H 3.91) and C-8 (δ_C 153.9). The methylenedioxy moiety was placed at C-3' / C-4' (δ_C 148.9) of ring B, which has an AXY-spin system with protons at δ_H 7.03 (d, J = 1.7 Hz, H-2'), δ_H 6.97 (dd, J =1.6, 8.0 Hz, H-6') and δ_H 6.84 (d, J = 8.0 Hz, H-5'). The isoflavone is also substituted with four glycosides as indicated by the characteristic signals of four anomeric protons at δ_H 5.08, 4.77, 4.73 and 4.55. Two of the sugars that possessed methyl groups at δ_H/δ_C 1.14/17.9 and δ_H/δ_C 1.09/17.8, respectively, and were assigned as rhamnosyl, whereas the other two as glucosyl. The ^{1}H and ^{13}C NMR signals corresponding to each sugar (**Table 2**) were identified with the help of COSY, TOCSY, HSQC, HMBC and NOESY spectra (Figures S26-S30, Supporting Information). Carbon C-6 of the isoflavone is the site of *O*-glycosidation, based on the NOE of H-5 (δ_H 7.13) and OMe-7 (δ_H 3.80) with the anomeric proton H-1' (δ_H 5.05) of the first glucose as well as on the HMBC of H-1'' and C-6 (δ_C 157.0). The large coupling constant, $^3J_{H1'\,H2'}$ = 7.9 Hz of the anomeric proton H-1' (δ_H 5.05) to H-2'' (δ_H 3.78) suggested the β-linkage of the sugar to the isoflavone.[42] The large diaxial coupling constants of the protons of this sugar moiety (**Table 2**) suggested it to be a β-glucose. Both H-1''' (δ_H 4.53), the anomeric proton of the second sugar moiety, and H-2' (δ_H 3.80) showed HMBC with C-4' (δ_C 89.4) that together with the NOE of H-4' (δ_H 3.61) and H-1' (δ_H 4.53) and with the $^3J_{H1'\,H2'}$ = 7.8 Hz identified the β-glucopyranosyl-(4' →1')-β-glucopyranosyl linkage between the two glycoside moieties. The characteristic large diaxial coupling constants (**Table 2**) and the NOEs of H-1''' (δ_H 4.53) with 1'''' (δ_H 4.74), H-3'''' (δ_H 3.70) and H-3'''' (δ_H 3.80) indicated the second sugar moiety to also be a β-glucopyranosyl. The anomeric protons of the two rhamnosyl moieties, H-1'' (δ_H 4.71) and H-1'' (δ_H 4.74), showed HMBC with C-7' (δ_C 67.8) and C-7' (δ_C 68.6), respectively. Furthermore, H-7' (δ_H 4.08 and 3.58)

[a] The CC_{50} assay was complemented by microscopic recording of possible cytostatic activity of test compounds manifested as poor cell proliferation (PCP), altered cell shape (ACS) or poor cell staining (PCS). [b] SI of 1 indicates lack of antiviral activity i.e., lack of the cell protection against RSV; SI of 2-10 suggests that antiviral activity may at least in some compounds be unspecific due to cytostatic activity (poor cell proliferation/altered cell shape) that occurs at concentrations just below the CC_{50} and may not be detectable by cell toxicity assay used; SI > 10 suggests specific antiviral activity for most compounds tested. [c] ND, Not determined

and H-7' (δ_H 4.04 and 3.55) showed HMBC to the respective anomeric carbons of the rhamnosyl groups, C-1' (δ_C 102.1) and C-1'' (δ_C 102.4). These HMBCs along with the NOEs of H-7' (δ_H 4.11 and 3.60) and H-7' (δ_H 4.06 and 3.58) to H-1'' (δ_H 4.71) and H-1'' (δ_H 4.74), respectively established the α-rhamnosyl-(1'' →7')-β-glucosyl and the α-rhamnosyl-(1'' →7')-β-glucosyl linkages. The equatorial orientation of H-1'' (δ_H 4.71) and H-1'' (δ_H 4.74) was assigned upon the observation of characteristic small, diequatorial $^3J_{H1''\,H2''}$ = 1.2 Hz and $^3J_{H1''\,H2''}$ = 1.4 Hz coupling constants and of the absence of NOEs between H-1'' (δ_H 4.74) and H-3''' (δ_H 3.80) and H-1''' (δ_H 4.74) and H-3'' (δ_H 4.80). The identity of the aglycone was further confirmed by comparison of its NMR data with that of its literature known 6-methoxy derivative (Figures S33-S39).[43] The absolute configuration of compound **4** has not

Table 2. NMR Spectroscopic Data (^{1H} 800 and ^{13C} 200 MHz, CD_3OD) for Obloneside (4)

position	δ_C, type	δ_H *m* (*J* in Hz)	HMBC
2	154.2, CH	8.17 s	C-1' , C-3, C-4, C-8a
3	126.9, C		
4	177.1, CO		
4a	115.2, C		
5	101.8, CH	7.12 s	C-4, C-4a, C-6, C-7, C-8a
6	157.0, C		
7	142.1, C		
8	153.9, C		
8a	155.5, C		
1'	126.0, C		
2' -	110.8, CH	7.03 d (1.7)	C-3, C-3' , C-4' , C-6'
3'	148.9, C		
4'	148.9, C		
5'	109.0 ,C	6.84 d (8.0)	C-1' , C-3' , C-4'
6'	123.8, CH	6.97 dd (8.0, 1.7)	C-2' , C-3, C-4'
OCH_2O	102.5, CH_2	5.98 d (1.2)	C-3' , C-4'
OMe-7	62.8, OMe	3.92 s	C-7
OMe-8	62.3, OMe	3.91 s	C-8
β-glycoside moiety 1			
1'	101.6, CH	5.05 d (7.9)	C-3' , C-5' , C-6
2'	73.6, CH	3.78 dd (8.7, 7.9)	C-1″, C-4″
3'	76.7, CH	3.70 dd (9.5, 7.9)	C-4″, C-5″, C-7″
4'	89.4, CH	3.61 dd (9.5, 9.1)	C-1' , C-2″, C-3‴
5'	70.2, CH	3.46 dd (9.3, 9.1, 7.3)	C-1″, C-3″, C-4″, C-7″
7'	67.8, OCH_2	4.08 d (9.3)	C-1' ' , C-2″, C-4″, C-5″
		3.58 (7.3)	
β-glycoside moiety 2			
1'	105.4, CH	4.53 d (7.8)	C-3' , C-4' , C-5‴
2'	75.2, CH	3.34 dd (8.9, 7.8)	C-1‴, C-5‴
3'	76.6, CH	3.55 dd (9.7, 8.9)	C-2‴, C-4‴
4'	71.7, CH	3.32 dd (9.7, 9.7)	C-3‴, C-5‴, C-7‴
5'	77.6, CH	3.43 ddd (9.7, 9.2, 7.2)	C-1‴, C-3‴, C-4‴, C-7‴
7'	68.5, OCH_2	4.04 d (9.2)	C-1' ' , C-2⁗, C-4‴
		3.58 d (7.2)	
α-rhamnoside moiety 3			
1' '	102.1, CH	4.71 d (1.2)	C-2⁗, C-3⁗, C-5⁗, C-7'
2' '	71.9, CH	3.90 dd (3.3, 1.2)	C-1⁗, C-3⁗, C-4⁗
3' '	72.2, CH	3.70 dd (9.4, 3.3)	C-4⁗, C-5⁗
4' '	74.1, CH	3.37 dd (9.5, 9.4)	C-2⁗, C-3⁗, C-5⁗
5' '	70.0, CH	3.67 dd (9.5, 6.2)	C-1⁗, C-3⁗, C-4⁗
7' '	18.1, CH_3	1.28 d (6.2)	C-4⁗, C-5⁗
α-rhamnoside moiety 4			
1' '	102.4, CH	4.74 d (1.4)	C-2⁗, C-3⁗, C-5⁗, C-7'
2' '	72.0, CH	3.92 dd (3.4, 1.4)	C-1⁗, C-4⁗
3' '	72.4, CH	3.80 dd (9.4, 3.4)	C-1⁗, C-2⁗, C-4⁗
4' '	74.0, CH	3.39 dd (9.5, 9.4)	C-2⁗, C-3⁗, C-5⁗
5' '	69.9, CH	3.63 dd (9.5, 6.2)	C-1⁗, C-3⁗, C-4⁗
7' '	18.0, CH_3	1.21 d (6.2)	C-4⁗, C-5⁗

been elucidated. However, natural sugars are known to almost always be D-glucose and L-rhamnose.[44,45] Based on the above spectroscopic data, obloneside (**4**) was characterized as isoplatycarpanetin-6-*O*-β-glucosyl-(7' →1' ')-α-rhamnosyl-(4' →1' ')-β-glucosyl-(7' →1' ')-α-rhamnoside.

The extracts and the isolated compounds were tested for antiviral activity against RSV by the viral plaque reduction assay in cultures of human laryngeal epidermoid carcinoma (HEp-2) cells (Table 3, Supporting Information). A tetrazolium-based cytotoxicity assay on HEp-2 cells was also performed to exclude that the anti-RSV activity was a result of general cytotoxicity. The cytotoxicity assay was complemented by microscopy observation of the compound/extract-treated cells to detect possible cytostatic activity, such as poor cell growth and/or altered cell shape that may affect antiviral activity. The leaf extract exhibited anti-RSV activity with IC_{50} of 0.7 μg/mL and comparably low toxicity, CC_{50} of 50.0 μg/mL, for HEp-2 cells (Table 3 and Figures S129-S130, Supporting Information), whereas the root wood extract showed anti-RSV activity with IC_{50} of 3.4 μg/mL. Both crude extracts decreased the cell viability also at concentrations lesser than their CC_{50} values (Figure S130, Supporting Information), suggesting that they are rich in

Table 3. Anti-RSV activity, cytotoxicity for HEp-2 cells, and selectivity indices (SI) of compounds isolated from *Milletia oblata*

Compound/extract	Anti-RSV activity IC_{50} (μM)	Cytotoxicity CC_{50} (μM)	Cytostatic activity[a]	SI (CC_{50}/IC_{50})
1	>100.0	>100.0		1.0
2	>100.0	>100.0		1.0
3	22.0	90.0		4.1
4	>100.0	>100.0		1.0
5	53	>100.0		>1.9
6	1.4	50.0	PCS (20.0 μM)	35.7
7	1.8	6.7		3.8
8	1.5	42.0	PCS (20.0 μM)	28.0
9	0.8	12.5	PCS (0.8 and 4.0 μM)	15.6
10	0.4	26.5	PCS (4.0 μM)	61.6
11	8.0	91.0	PCS (20.0 μM)	11.4
12	>100.0	>100		1.0
13	2.1	>100.0	PCS (4.0, 20.0 and 100.0 μM)	>47.6
14	10.0	>100.0	PCS (100.0 μM)	>10
15	10.0	65.0	PCS (20.0 μM)	6.5
16	>100.0	>100.0		1.0
17	>100.0	>100.0		1.0
18	ND[c]	ND[c]	ND[c]	ND[c]
19	>0.8	2.0		<2.5
Ribavirin	10.6	>100	PCP (100 μM)	>9.4
DMSO	>100	>100		1

cytotoxic/cytostatic compounds that may interfere with their anti-RSV activities (Figure S129, Supporting information). Out of the nineteen isolated compounds tested, **6** (IC_{50} 1.4 μM), **8** (IC_{50} 1.5 μM), **10** (IC_{50} 0.4 μM), **11** (IC_{50} 8.0 μM), and **14** (IC_{50} 10.0 μM) exhibited substantial anti-RSV activity, and showed cytotoxicity (26.5 μM to >100.0 μM) and cytostatic activity only at much higher concentrations than their antiviral IC_{50} values (Table 3 and Figures S131-S132, Supporting Information). Compounds **9** (IC_{50} 0.8 μM) and **13** (IC_{50} 2.1 μM) showed substantial anti-RSV activity with selectivity indices (SI) of 15.6 and >47.6, respectively; however, both exhibited cytostatic activity at concentrations close to their IC_{50} values (Table 3). At this stage, it is difficult to assess whether the cytostatic activity of these specific compounds contributed to the protection of cells against virus infection and accordingly the specificity of anti-RSV action of **9** and **13** requires further investigation. An attempt was made to address this issue by testing cytotoxic activities of the most promising compounds in human embryonic lung fibroblasts (HELF), i.e., primary cells derived from lung interstitium. In these cells, the CC_{50} values were >100 μM for compounds **3**, **11**, **14**, and 47.1 μM for compound **15**, thus confirming the low cytotoxic activity of these compounds found in HEp-2 cells (Table 3), an observation that further strengthen their antiviral potential. In contrast the other active compounds showed CC_{50} values at low concentrations, i.e. 1.3 μM for **6**, 4.8 μM for **8**, 0.3 μM for **10**, and 9.0 μM for **13**, indicating that these compounds were more toxic for HELF cells than for HEp-2 cells, and the specificity of their anti-RSV activity requires further studies in HELF cells. The addition of the same volume of pure DMSO as the volume of the solution of the studied compounds was used as a negative control in this study, while ribavirin, the only antiviral drug approved in form of aerosol formulations for the treatment of RSV disease, was used as a positive control. In our hands, ribavirin inhibited RSV infection of HEp-2 cells with IC_{50} of 10.6 μM, and was not toxic for cells at concentrations up to 100.0 μM (CC_{50}>100.0 μM), but showed cytostatic activity at 100.0 μM (Table 3 and Figure S131-S132, Supporting Information).

We also tested the crude extracts and the isolated compounds for their capability to inhibit the human rhinovirus 2 (HRV-2) infection of adenocarcinoma cells of the uterine cervix (HeLa). Compound **3** displayed anti-HRV-2 activity by protecting the cells at IC_{50} of 4.2 μM while showing toxicity for HeLa cells first at CC_{50} of 48.0 μM (SI 11.4, Figure S133, Supporting Information). Compound **3** also showed anti-RSV activity (IC_{50} 22.0 μM, Table 3 and Figures S131-S132, Supporting Information). Our observations emphasize the antiviral potential of rotenoids as some of these compounds were reported to inhibit the Newcastle disease virus and the herpes simplex virus (HSV),[46] and 12a-hydroxyrotenoids showed modest anti-HSV activity.[47] Isoflavonoids are believed to be produced by plants for protection against microbes, and they can therefore be expected to show activity against viruses.[48]

In conclusion, nineteen natural products, including three new roteinoids (**1**-**3**) and a new glycosylated isoflavone (**4**), were isolated from the CH_2Cl_2/MeOH (1:1) extract of the leaves and the root wood of *Millettia oblata* ssp. *teitensis.* The absolute configuration of rotenoids was for the first time determined by vibrational circular dichroism (VCD) spectroscopy. In addition to the crude extracts (IC_{50} 0.7 and 3.4 μg/mL), the isolated compounds oblarotenoid A (**6**), 12a-hydroxymunduserone (**8**), deguelin (**10**), ichthynone (**11**), and 4' -prenyloxyderrone (**14**) showed anti-RSV activity (IC_{50} 0.4 – 10.0 μM) with low cytotoxicities in HEp-2 cells (>26.5 μM). Tephrosin (**9**) and

isoerythrin-A-4' -prenyl ether (**13**) showed substantial anti-RSV activity, IC_{50} 0.8 and 2.1 μM), respectively yet also exhibited cytostatic activity (CC_{50} 12.5 and >100.0 μM). Besides its anti RSV activity (IC_{50} 22.0 μM), 9-methoxy-2,3-methylenedioxy-6a-2a-dehydrorotenoid (**3**) protected cells from HRV-2 infection (IC_{50} of 4.2 μM) whereas showing low cytotoxicity (CC_{50} of 48.0 μM).

EXPERIMENTAL SECTION

General experimental procedures. Optical rotations were measured on Perkin Elmer 341-LC instrument. NMR spectra were acquired on an Agilent MR-400-DD2 spectrometer equipped with a 5 mm OneNMR probe, on a Bruker Avance Neo 500 MHz or Bruker Avance NEO 800 MHz instrument equipped with a 5 mm cryogenic TXO probe. The spectra were processed using the MestReNova 14.1 software and were referenced to the residual solvent peak. LC-ESIMS data were acquired on a Waters Micromass ZQ Multimode Ionization electrospray ionization (ESI) connected to an Agilent 1100 series gradient pump system and a C_8 column (Gemini), using Milli-Q H_2O/MeCN (5:95 to 95:5, with 1% HCO_2H over 4 min) eluent mixture. HRESIMS spectra were acquired with a Q-TOF LC/MS spectrometer with a lock mass-ESI source (Stenhagen Analysis Lab AB, Gothenburg, Sweden), using a 2.1 x 30 mm 1.1 μm reverse phase $^{49}C_{18}$ column and H_2O-MeCN gradient (5:95 to 95:5, with 0.2% HCO_2H). TLC analyses were carried out on Merck pre-coated silica gel 60 F_{254} plates. Preparative TLCs were performed on glass plates of 20 × 20 cm dimension, pre-coated with silica gel 60F_{254} having 0.25 to 1 mm thickness. Column chromatography was performed on silica gel (40-63 μm mesh), and gel filtration on Sephadex™ LH-20.

Plant Materials. The root wood and the leaves of *Millettia oblata* ssp. *teitensis* were collected in July 2014 from Ngaongao forest, Taita Hill, Taita County, Kenya, and were assigned the voucher number TD-04/2014. The plant was identified by Mr. Patrick Chalo Mutiso of the Department of Biology, University of Nairobi, Kenya, where the specimen was deposited.

Extraction and Isolation. The dried and ground leaves of *Millettia oblata* (795 g) were extracted with CH_2Cl_2/MeOH (1:1) (4 x 1.5 l) for 24 h by cold percolation. The extract was filtered and the supernatant was concentrated under reduced pressure to obtain the extract (35 g). A portion of this crude extract (27 g) was subjected to column chromatography on silica gel (300 g) using *iso*-hexane (a mixture of isomeric branched chain hexanes) containing increasing amounts of EtOAc to give a total of 100 fractions. The first 30 fractions eluted with 0-3% EtOAc in *iso*-hexane were not further investigated. Fractions 31-40 eluted with 6% EtOAc in *iso*-hexane were combined, based on their TLC profile and were subjected to column chromatography on Sephadex LH-20 (CH_2Cl_2/MeOH, 1:1) to give oblarotenoid C (**5**, 8 mg) and 9-methoxy-2,3-methylendioxy-6a-12a-dehyrorotenoid (**3**, 10 mg). Fractions 41-48 eluted at 7% EtOAc in *iso*-hexane afforded a white precipitate, which was washed with MeOH to afford oblarotenoid A (**6**, 11 mg). Fractions 49-57 eluted with 8% EtOAc in *iso*-hexane showed the presence of five compounds by TLC analysis, and were separated by column chromatography on silica gel (eluent: *iso*-hexane/CH_2Cl_2; 1:1) to yield an additional amount of oblarotenoid A (**6**, 2 mg) together with 12a-hydroxymunduserone (**8**, 4 mg), tephrosin (**9**, 7 mg), deguelin (**10**, 10 mg) and a mixture, which was further separated by column chromatography over silica gel (eluent; *iso*-hexane/CH_2Cl_2/EtOAc: 60:35:10) to afford deguelin (**10**, 2 mg) and (6aS,12aS)-4,9-dimethoxy-2,3-methylenedioxyrotenoid (**1**, 3 mg). The fractions eluted with 10-14% EtOAc gave a mixture of four compounds, which was further purified on Sephadex LH-20 eluting with CH_2Cl_2/MeOH (1:1) to yield 7,2',5'-trimethoxy-3',4'-methylenedioxyisoflavone (**12**, 10 mg), oblarotenoid D (**7**, 8 mg) and a fraction containing three compounds. These three compounds were separated by preparative TLC developed in a mixture of *iso*-hexane/CH_2Cl_2/EtOAc (13:5:2) to yield ichthynone (**11**, 4 mg), oblarotenoid D (**7**, 1 mg) and (6a*R*,12a*R*)-9,10-dimethoxy-2,3-methylenedioxyrotenoid (**2**, 4 mg).

The root wood (800 g) was extracted to give a light brown crude extract (30 g) and was subjected to column chromatography over silica (300 g) eluting it as described above. The fractions eluted with 4-8% EtOAc in *iso*-hexane afforded isoerythrin-A-4' (**13**, 7 mg), 4'-prenyloxyderrone (**14**, 15 mg), and a mixture of two compounds, which were separated on Sephadex LH-20 (CH_2Cl_2/MeOH, 1:1) to give cuneatin methyl ether (**15**, 6 mg) and calopogonium isoflavone B (**16**, 10 mg). The fractions eluted with 10% EtOAc were further purified on Sephadex LH20 to yield isobavachromene (**19**, 11 mg). Fractions eluted with 12-18% EtOAc in *iso*-hexane afforded a mixture of two compounds, which upon purification by column chromatography over silica gel (*iso*-hexane:/CH_2Cl_2, 1:1) yielded maximaisoflavone G (**17**, 9 mg) and milldurone (**18**, 8 mg). The fractions eluted with 100% EtOAc were further purified by chromatography Sephadex LH-20 (100% MeOH) and yielded obloneside (**4**, 15 mg).

(6aS,12aS)-2,9-Dimethoxy-3,4-methylenedioxyrotenoid (***1***): White solid; $[\alpha]^{20}_D$ +44.0 (*c* 0.2 CH_3OH); UV λ_{max} (log ') 280 nm (4.2) and 305 nm (4.0); ^1H and ^{13}C NMR, see **Table 1** and Figures S1-S9, Supporting Information; HRESIMS *m/z* 357.0976 $[M+H]^+$ (calcd 357.0974 for $C_{19}H_{17}O_7$).

(6aR,12aR)-9,10-Dimethoxy-2,3-methylenedioxyrotenoid (***2***): White solid, $[\alpha]^{20}_D$ +42.0 (*c* 0.3 CH_3OH); UV λ_{max} (log ϵ) 285 nm (4.3) and 305 nm (3.9); ^1H and ^{13}C NMR, see **Table 1** and Figures S10-S17, Supporting Information; HRESIMS *m/z* 355.0354 $[M+H-H_2O]^+$ (calcd for $C_{19}H_{15}O_7$ 355.0815), LC-ESIMS m/z 373.2 $[M+1]^+$ (calcd 373.1 for $C_{19}H_{18}O_9$).

9-Methoxy-2,3-methylenedioxy-6a,2a-dehydrorotenoid (***3***): White solid; UV λ_{max} (log ϵ) 237 nm (4.5), 278 nm (2.3), and 310 nm (4.0); ^1H and ^{13}C NMR, see **Table 1** and Figures S18-S24, Supporting Information; HRESIMS *m/z* 325.074 $[M+H]^+$ (calcd 325.0712 for $C_{18}H_{13}O_6$).

Obloneside (***4***): White solid; UV λ_{max} (log ϵ) 290 nm (4.3); ^1H and ^{13}C NMR, see **Table 2** and Figures S25-S32, Supporting Information; HRESIMS *m/z* 959.3043 $[M+H]^+$ (calcd 959.3033 for $C_{42}H_{55}O_{25}$).

Cells and viruses. Human laryngeal epidermoid carcinoma (HEp-2) cells were cultivated in Dulbecco's Modified Eagle's Medium (DMEM) supplemented with 8% fetal calf serum and 292 μg/mL of L-glutamine. Human adenocarcinoma cells of uterine cervix (HeLa) cells were grown in Eagle´s minimum essential medium supplemented with 5% fetal calf serum and antibiotics. Human embryonic

lung fibroblasts (HELF) were grown in Eagle´s minimum essential medium supplemented with 5% fetal calf serum, L-glutamine and antibiotics. The A2 strain of human respiratory syncytial virus (RSV) (ATCC VR-1540) was used. The RSV stock was prepared and stored as described previously by Lundin, et al. [50] In some experiments, strain HGP of human rhinovirus 2 (HRV-2) (ATCC, VR-482) was used.

Antiviral assays. The RSV plaque reduction assay was performed as described previously with some modifications. Briefly, the test extracts and compounds were serially diluted at a range of 1.6-200 µg/mL and 0.16-100 µM respectively in DMEM supplemented with 2% heat-inactivated fetal calf serum, 60 µg/mL of penicillin, 100 µg/mL of streptomycin, and 292 µg/mL of *L*-glutamine (DMEM-M), and then added to one-day-old cultures of HEp-2 cell in 24-well cluster plates. Following 15 min of incubation at 37 °C in a humidified atmosphere comprising 5% CO_2 (incubator), the cells were inoculated with 50–100 plaque-forming units (PFU) of RSV A2. After incubation of the virus-compound mixture with cells for 2.5 h in the CO_2 incubator, the inoculum was removed and 750 µl of 1% methylcellulose solution in DMEM-M comprising the same concentration of test compound/extract was added and left for a further three days in the CO_2 incubator. The cells were stained with a 1% solution of crystal violet, and the viral plaques were counted under a microscope. Ribavirin, a drug approved for the treatment of RSV disease, was used as a positive control whereas DMSO at concentrations corresponding to these present in the test compounds was used as solvent control.

The anti-HRV-2 activity of extracts and compounds was assessed by a tetrazolium-based colorimetric assay [52] with some modifications. Briefly, serial five-fold dilutions of test samples (0.16 -100 µM) in EMEM supplemented with 2% fetal calf serum, 1% pest stock, 1% *L*-glutamine stock, 30 mM $MgCl_2$, and 20 mM HEPES (pH 7.1) (EMEM-M) were added to one-day-old cultures of HeLa cells seeded in 96 well cluster plates. Following the incubation of cells with test samples for 3 h at 34°C CO_2 incubator, 100 tissue culture infectious doses ($TCID_{50}$) in EMEM-M were added. In some wells addition of the test samples and the virus was omitted to serve as the virus control and uninfected cell control respectively. After incubation of the test plates in the CO_2 incubator for 3 days, the CellTiter 96 Aqueous one solution reagent (Promega, Madison, WI, USA) was added, and following further incubation of plates in the CO_2 incubator for 1 h, the absorbance was recorded at 490 nm. The % of the test sample protection of cells against HRV-2 infection was calculated as (Absorbance of the test sample-virus control) ×100 / Absorbance of the cell control-virus control.

The cell toxicity assay. The tetrazolium-based cytotoxicity assay using a CellTiter 96 Aqueous one solution reagent (Promega, Madison, WI, USA) was performed for the test extracts and isolated compounds in HEp-2, HELF, and HeLa cells as described previously.[50]

Optical spectroscopy. UV absorbance and ECD spectra were collected simultaneously on a 0.02 mg/mL sample in MeOH using a path length of 10 mm on a ChiraScan-plus (Applied Photophysics) with a scan speed of 30 nm/min under a continuous N_2-flow. The solvent spectra were recorded under identical conditions to remove solvent bands in the UV spectra, and to baseline correct the ECD spectra. IR and VCD spectra were recorded simultaneously on a ChiralIR-2X (Biotools) equipped with a dual PEM system running at resolution of 4 cm^{-1} and the central PEM frequency set to 1400 cm^{-1}. Samples were dissolved in $CDCl_3$, and a cell equipped with BaF_2 windows and a path length of 100 µm and a total of 96000 scans were recorded (32 h). The final experimental VCD spectra were obtained by subtracting the solvent VCD spectrum recorded under identical conditions.

Calculations. A low energy conformation library of postulated compounds **1** and **2** in both the *cis* and *trans* configuration were created using PCModel [53] with the incorporated MMFF94 force field. All conformers within a cut-off of 5 kcal/mol from the lowest energy conformer were retained and subjected to DFT optimization and spectral calculations at the B3LYP/6-311++G(d,p) level of theory. DFT calculations were performed on conformers exhibiting a Boltzmann weight higher than 1% (based on Enthalpy). The solvent was implicitly taken into account using the IEFPCM model as implemented in the Gaussian suite. All DFT level calculations were performed using the Gaussian 16 software package [54] with tight convergence criteria and ultrafine integration grids. For each conformer IR absorbance and VCD spectra were created by applying a Lorentzian broadening with full half width at half maximum of 10 cm^{-1} and subsequent Boltzmann weighted based on their enthalpies. To compare the calculated spectra with the experimental one, a spectrascaling factor of 0.98 was applied on the calculated frequencies.

ASSOCIATED CONTENT

We thank the Swedish Research Council (No. 2019-03715 to ME and No. 2021-06386 and 2018-03918 to TB) for financial support. We are grateful to Mr. P.C. Mutiso of Herbarium, Botany Department, University of Nairobi, for the identification of the plant species for the study, and to Dawson McCall and Yasin Katwere for their support to Ivan Kiganda at the initial stage of this work.

For Table of Contents Only

Notes

1. **Data Availability Statement.** The original FIDs and MestreNova files for all compounds, NMReDATA [55-56] files and CSEARCH [30] results for the news compounds **1-4**, original UV and IR spectra, and DFT computed conformers for compounds **1** and **2** are freely available on Zenodo (DOI: 10.5281/zenodo.10846050)

2. Supporting information. The following file is available free of charge.

NMR, MS and optical spectroscopy data for the isolated compounds and antiviral activity and cytotoxicity data (PDF)

3.

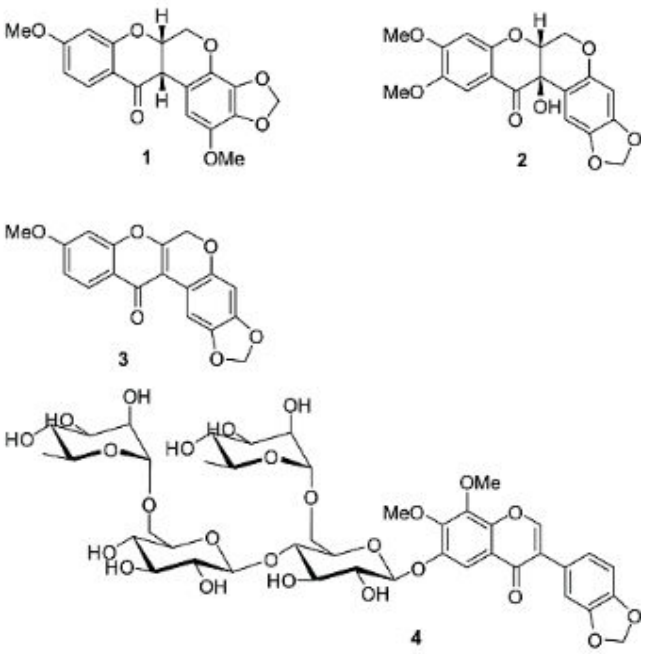

Notes

The authors declare no conflict of interest.

REFERENCES

1) Christy, M. P.; Uekusa, Y.; Gerwick, L.; Gerwick, W. H. Natural Products with Potential to Treat RNA Virus Pathogens Including SARS-CoV-2. J Nat Prod 2021, *84* (1), 161–182. https://doi.org/10.1021/acs.jnatprod.0c00968.

2) Clercq, E.; Li, G. Clin. Microbiol. Rev 2016, 29, 695–747.

3) Boldogh, I.; Albrecht, T.; Porter, D. D. Persistent Viral Infections. 1996.

4) Cheng, V. C.-C.; Chan, J., F,-W,; Hung, I. F. N.; Yiuen; K-Y. Elsevier, 2016.

5) Ghoran, S. H.; Mohamed, E.-S.; Nazim, S.; Anake, K. Molecules 2021, 26, 3–28.

6) Sampath, S.; Khedr, A.; Qamar, S.; Tekin, A.; Singh, R.; Green, R.; Kashyap, R. C. 2021, 13, e18136.

7) Assari, S.; Boyce, S.; Bazargan, M.; Caldwell, C. H.; Mincy, R. Maternal Education at Birth and Youth Breakfast Consumption at Age 15: Blacks' Diminished Returns. *J (Basel)* 2020, 3 (3), 313–323. https://doi.org/10.3390/j3030024.

8) Zakaryan, H.; Arabyan, E.; Adrian, O.; Keivan, Z. A. Virol 2017, 162, 2539–2551.

9) Wang, L.; Song, J.; Liu, A.; Xiao, B.; Li, S.; Wen, Z.; Lu, Y.; Du, G. Research Progress of the Antiviral Bioactivities of Natural Flavonoids. Nat Prod Bioprospect 2020, 10 (5), 271–283. https://doi.org/10.1007/s13659-020-00257-x.

10) Jo, S.; Kim, S.; Shin, D. H.; Kim, M. S. J. Enzyme Inhib. Med. Chem 2020, 35, 145–151.

11) Jucá, M. M.; Cysne Filho, F. M. S.; de Almeida, J. C.; Mesquita, D. da S.; Barriga, J. R. de M.; Dias, K. C. F.; Barbosa, T. M.; Vasconcelos, L. C.; Leal, L. K. A. M.; Ribeiro, J. E.; Vasconcelos, S. M. M. Flavonoids: Biological Activities and Therapeutic Potential. Nat Prod Res 2020, 34 (5), 692–705. https://doi.org/10.1080/14786419.2018.1493588.

12) Jena, R.; Rath, D.; Rout, S. S.; Kar, D. M. A Review on Genus *Millettia*: Traditional Uses, Phytochemicals and Pharmacological Activities. Saudi Pharm J 2020, 28 (12), 1686–1703. https://doi.org/10.1016/j.jsps.2020.10.015.

13) Gomes, G. d S.; Silva, G. S.; Domingos, L. d S. S.; Regiglaucia, R. d O.; Gonçalo, M. d. C. Asian J. Environ. Ecology 2018, 4, 1–10.

14) Chen, K.; Tang, H.; Zheng, L.; Wang, L.; Xue, L.; Peng, A. -h; Tang, M. -h; Long, C.; Chen, X.; Ye, H. -y; Chen, L. -j. Identification of Compounds with Cytotoxic Activity from Millettia Dorwardi Coll. Et. Hemsl. Phytochemistry Letters 2018, 25, 60–64. https://doi.org/10.1016/j.phytol.2018.03.004.

15) Raksat, A.; Maneerat, W.; Andersen, R. J.; Pyne, S. G.; Laphookhieo, S. Antibacterial Prenylated Isoflavonoids from the Stems of *Millettia Extensa* . *J. Nat. Prod* 2018, 81 (8), 1835–1840. https://doi.org/10.1021/acs.jnatprod.8b00321.

16) Banzouzi, J. T.; Prost, A.; Rajemiarim, M.; Ongoka, P. Traditional Uses of the African Millettia Species (Fabaceae). *International J. of Botany* 2008, 4 (4), 406–420. https://doi.org/10.3923/ijb.2008.406.420.

17) Yenesew, A.; Jacob, O. M.; Peter, G. W. P. 1998, 9, 295–300.

18) Deyou, T.; Marco, M.; Heydenreich, M.; Pan, F.; Gruhonjic, A.; Fitzpatrick, P. A.; Koch, A.; Derese, S.; Pelletier, J.; Rissanen, K.; Yenesew, A.; Erdélyi, M. Isoflavones and Rotenoids from the Leaves of *Millettia Oblata* Ssp. *Teitensis* . *J. Nat. Prod* 2017, 80 (7), 2060–2066. https://doi.org/10.1021/acs.jnatprod.7b00255.
19) Derese, S.; Barasa, L.; Akala, H. M.; Yusuf, A. O.; Kamau, E.; Heydenreich, M.; Yenesew, A. P. L. 2014, 8, 69–72.
20) Zingue, S.; Tchoumtchoua, J.; Ntsa, D. M.; Sandjo, L. P.; Cisilotto, J.; Nde, C. B. M.; Winter, E.; Awounfack, C. F.; Ndinteh, D. T.; Clyne, C.; Njamen, D.; Halabalaki, M.; Creczynski-Pasa, T. B. BMC Complement Altern Med 2016, 16, 421.
21) Andres, A.; Donovan, S. M.; Kuhlenschmidt, M. S. Soy Isoflavones and Virus Infections. J Nutr Biochem 2009, 20 (8), 563–569. https://doi.org/10.1016/j.jnutbio.2009.04.004.
22) Kumar, P. K. P.; Priyadharshini, A.; Muthukumaran, S. M.-R. Med Chem 2021, 21, 1734–1746.
23) Carlson, D. G.; Weislede, D.; Tallent, W. H. Tetrahedron 1973, 29, 2731–2741.
24) Ren, Y.; Benatrehina, P. A.; Muñoz Acuña, U.; Yuan, C.; Chai, H.-B.; Ninh, T. N.; Carcache de Blanco, E. J.; Soejarto, D. D.; Kinghorn, A. D. Isolation of Bioactive Rotenoids and Isoflavonoids from the Fruits of Millettia Caerulea. Planta Med 2016, 82 (11–12), 1096–1104. https://doi.org/10.1055/s-0042-108059.
25) Daniel, B.; Yang, L. J.; Derese, S.; Ndakala, A.; Coghi, P.; Heydenreich, M.; Wong, V. K. W.; Moller, H. M.; Yenesew, A. Nat. Prod. Res 2021, 35, 2744–2747.
26) Pancharoen, O.; Athipornchai, A.; Panthong, A.; Taylor, W. C. Isoflavones and Rotenoids from the Leaves of Millettia Brandisiana. Chem. Pharm. Bull 2008, 56 (6), 835–838. https://doi.org/10.1248/cpb.56.835.
27) Veitch, N. C.; Sutton, P. S. E.; Kite, G. C.; Ireland, H. E. Six New Isoflavones and a 5-Deoxyflavonol Glycoside from the Leaves of *Ateleia H Erbert-Smithii* . *J. Nat. Prod* 2003, 66 (2), 210–216. https://doi.org/10.1021/np020425u.
28) Marco, M.; Deyou, T.; Gruhonjic, A.; Holleran, J.; Duffy, S.; Heydenreich, M.; Firtzpatrick, P. A.; Landberg, G.; Koch, A.; Derese, S.; Pelletier, J.; Avery, V. M.; Erdélyi, M.; Yenesew, A. Pterocarpans and Isoflavones from the Root Bark of Millettia Micans and of Millettia Dura. Phytochemistry Letters 2017, 21, 216–220. https://doi.org/10.1016/j.phytol.2017.07.012.
29) Ma, S.; Huang, Y.; Zhao, Y.; Du, G.; Feng, L.; Huang, C.; Li, Y.; Guo, F. P. L. 2016, 16, 213–218.
30) ()Robien. W. Molecules 2021, 26, 3413.
31) Yenesew, A.; Irungu, B.; Derese, S.; Midiwo, J. O.; Heydenreich, M.; Peter, M. G. Two Prenylated Flavonoids from the Stem Bark of Erythrina Burttii. Phytochemistry 2003, 63 (4), 445–448. https://doi.org/10.1016/s0031-9422(03)00209-7.
32) Bhandari, P.; Crombie, L.; Sanders, M.; Whiting, D. A. Chem. Commun 1988, 1085–1086.
33) Panichpol, K.; Waterman, P. G. P. 1978, 17, 1363–1367.
34) Marais, J. P. J.; Ferreira, D.; Slade, D. Stereoselective Synthesis of Monomeric Flavonoids. *Phytochemistry* 2005, 66 (18), 2145–2176. https://doi.org/10.1016/j.phytochem.2005.03.006.
35) Unai, T.; Yamamoto, I. Agr Biol Chem Tokyo. 1973, 37, 897–901.
36) Starks, C. M.; Williams, R. B.; Norman, V. L.; Lawrence, J. A.; Goering, M. G.; O'Neil-Johnson, M.; Hu, J.-F.; Rice, S. M.; Eldridge, G. R. Abronione, a Rotenoid from the Desert Annual Abronia Villosa. *Phytochemistry Letters* 2011, 4 (2), 72–74. https://doi.org/10.1016/j.phytol.2010.08.004.
37) Kostova, I.; Ognyanov, I. Monatsh Chem. 1986, 117, 689–693.
38) Tozatti, C. S. S.; Khodyuk, R. G. D.; da Silva, A. O.; Dos Santos, E. D. A.; de Lima, M. S. do A. E. D. P.; Hamel, E. SYNTHESIS AND BIOLOGICAL EVALUATION OF BIARYL ANALOGS OF ANTITUBULIN COMPOUNDS. *Quim Nova* 2012, 35 (9), 1758–1762. https://doi.org/10.1590/S0100-40422012000900010.
39) Meesakul, P.; Suthiphasilp, V.; Teerapongpisan, P.; Rujanapun, N.; Chaiyosang, B.; Tontapha, S.; Phukhatmuen, P.; Maneerat, T.; Charoensup, R.; Duangyod, T.; Patrick, B. O.; Andersen, R. J.; Laphookhieo, S. P. Rotenoids and Isoflavones from the Leaf and Pod Extracts of Millettia Brandisiana Kurz. *Phytochemistry* 2022, 204, 113440. https://doi.org/10.1016/j.phytochem.2022.113440.
40) Silva, B. P.; Bernardo, R. R.; Parente, J. P. Rotenoids from Roots of Clitoria Fairchildiana. *Phytochemistry* 1998, 49 (6), 1787–1789. https://doi.org/10.1016/S0031-9422(98)00235-0.
(41) Miyano, M. *J. Org. Chem.* **1969**, *35*, 246-249.
(42) Szeja, W.; Grynkiewicz, G.; Rusin, A. *Curr. Org. Chem.* **2017**, *21*, 218-235.
(43) Torrance, S. J.; Wiedhopf, R. M.; Hoffmann, J. J.; Cole, J. R. *Phytochemistry* **1979**, *18*, 366-368.
(44) Szarek, W. A.; Hay, G. W.; Vyas, D. M.; Ison, E. R.; Hronowski, L. J. J. *Can. J. Chem.* **1984**, *62*, 671-674.
(45) Pikuta, E. V.; Hoover, R. B.; Klyce, B.; Davies, P. C. W.; Davies, P. *Instruments, Methods, and Missions for Astrobiology IX* **2006**, *6309*.
(46) Takatsuki, A.; Nobuji, N.; Makoto, M.; Gakuzo, T.; Masanao, M.; Kei, A.; Isamu, Y.; Tomomasa, M. *Appl. Microbiol.* **2002**, *18*, 660-667.
(47) Phrutivorapongkul, A.; Lipipun, V.; Ruangrungsi, N.; Watanabe, T.; Ishikawa, T. *Chem. Pharm. Bull.* **2002**, *50*, 534-537.
(48) Andres, A.; Donovan, S. M.; Kuhlenschmidt, M. S. *J. Nutr. Biochem.* **2009**, *20*, 563-9.

(49) Azani, N.; Babineau, M.; Bailey, C. D.; Banks, H.; Barbosa, A.; Pinto, R. B.; Boatwright, J.; Borges, L.; Brown, G.; Bruneau, A.; Candido, E.; Cardoso, D.; Chung, K.-F.; Clark, R.; Conceição, A. d.; Crisp, M.; Cubas, P.; Delgado-Salinas, A.; Dexter, K.; Doyle, J.; Duminil, J.; Egan, A.; De La Estrella, M.; Falcão, M.; Filatov, D.; Fortuna-Perez, A. P.; Fortunato, R.; Gagnon, E.; Gasson, P.; Rando, J. G.; Azevedo Tozzi, A. M. G. d.; Gunn, B.; Harris, D.; Haston, E.; Hawkins, J.; Herendeen, P.; Hughes, C.; Iganci, J. V.; Javadi, F.; Kanu, S. A.; Kazempour-Osaloo, S.; Kite, G.; Klitgaard, B.; Kochanovski, F.; Koenen, E. M.; Kovar, L.; Lavin, M.; Roux, M. l.; Lewis, G.; de Lima, H.; López-Roberts, M. C.; Mackinder, B.; Maia, V. H.; Malécot, V.; Mansano, V.; Marazzi, B.; Mattapha, S.; Miller, J.; Mitsuyuki, C.; Moura, T.; Murphy, D.; Nageswara-Rao, M.; Nevado, B.; Neves, D.; Ojeda, D.; Pennington, R. T.; Prado, D.; Prenner, G.; de Queiroz, L. P.; Ramos, G.; Ranzato Filardi, F.; Ribeiro, P.; Rico-Arce, M. d. L.; Sanderson, M.; Santos-Silva, J.; São-Mateus, W. B.; Silva, M. S.; Simon, M.; Sinou, C.; Snak, C.; de Souza, É.; Sprent, J.; Steele, K.; Steier, J.; Steeves, R.; Stirton, C.; Tagane, S.; Torke, B.; Toyama, H.; Cruz, D. T. d.; Vatanparast, M.; Wieringa, J.; Wink, M.; Wojciechowski, M.; Yahara, T.; Yi, T.; Zimmerman, E. *Taxon* **2017**, *66*, 44-77.

(50) Lundin, A.; Bergström, T.; Trybala, E. *Meth. Mol. Biol* **2013** *2013*, 345-363.

(51) Lundin, A.; Bergströma, T.; Bendrioua, L.; Kann, N.; Adamiak, B.; Trybala, E. *Antiviral Res.* **2010**, *88*, 317-324.

(52) Pauwels, R.; Balzarini, J.; Baba, M.; Snoeck, R.; Schols, D.; Herdewijn, P.; Desmyter, J.; De Clercq, E. *J. Virol. Meth.* **1988**, *20*, 309-321.

(53) Aerts, R.; Vanhove, J.; Herrebout, W.; Johannessen, C. *Chem. Sci.* **2021**, *12*, 5952-5964.

(54) Frisch, M. J. T., G. W.; Schlegel, H. B.; Scuseria, G. E.; Robb, M. A.; Cheeseman, J. R.; Scalmani, G.; Barone, V.; Petersson, G. A.; Nakatsuji, H.; Li, X.; Caricato, M.; Marenich, A. V.; Bloino, J.; Janesko, B. G.; Gomperts, R.; Mennucci, B.; Hratchian, H. P.; Ortiz, J. V.; Izmaylov, A. F.; Sonnenberg, J. L.; Williams-Young, D.; Ding, F.; Lipparini, F.; Egidi, F.; Goings, J.; Peng, B.; Petrone, A.; Henderson, T.; Ranasinghe, D.; Zakrzewski, V. G.; Gao, J.; Rega, N.; Zheng, G.; Liang, W.; Hada, M.; Ehara, M.; Toyota, K.; Fukuda, R.; Hasegawa, J.; Ishida, M.; Nakajima, T.; Honda, Y.; Kitao, O.; Nakai, H.; Vreven, T.; Throssell, K.; Montgomery, J. A., Jr.; Peralta, J. E.; Ogliaro, F.; Bearpark, M. J.; Heyd, J. J.; Brothers, E. N.; Kudin, K. N.; Staroverov, V. N.; Keith, T. A.; Kobayashi, R.; Normand, J.; Raghavachari, K.; Rendell, A. P.; Burant, J. C.; Iyengar, S. S.; Tomasi, J.; Cossi, M.; Millam, J. M.; Klene, M.; Adamo, C.; Cammi, R.; Ochterski, J. W.; Martin, R. L.; Morokuma, K.; Farkas, O.; Foresman, J. B.; Fox, D. J. *Gaussian 16, Revision C.01*, Gaussian, Inc.: Wallingford CT, 20156.

(55) Kuhn, S.; Wieske, L. H. E.; Trevorrow, P.; Schober, D.; Schlorer, N. E.; Nuzillard, J. M.; Kessler, P.; Junker, J.; Herraez, A.; Fares, C.; Erdelyi, M.; Jeannerat, D. *Magn Reson Chem* **2021**, *59*, 792-803.

(56) Pupier, M.; Nuzillard, J. M.; Wist, J.; Schlorer, N. E.; Kuhn, S.; Erdelyi, M.; Steinbeck, C.; Williams, A. J.; Butts, C.; Claridge, T. D. W.; Mikhova, B.; Robien, W.; Dashti, H.; Eghbalnia, H. R.; Fares, C.; Adam, C.; Kessler, P.; Moriaud, F.; Elyashberg, M.; Argyropoulos, D.; Perez, M.; Giraudeau, P.; Gil, R. R.; Trevorrow, P.; Jeannerat, D. *Magn Reson Chem* **2018**, *56*, 703-715.